Appl Phys A (2012) 106:941–947
DOI 10.1007/s00339-011-6714-4

Applied Physics A
Materials Science & Processing

Thermo-electric-induced dichroism in ion-exchanged glasses: a candidate mechanism for the alignment of silver nanoparticles

Arashmid Nahal · Razieh Talebi · MirFaez Miri

Received: 9 August 2011 / Accepted: 24 November 2011 / Published online: 16 December 2011

Abstract In the present work, the alignment mechanism of silver nanoparticles on the surface of a heated ion-exchanged glass, in presence of an external uniform DC electric field ($\vec{E}_0$) parallel to the surface of the sample, is studied. At high temperature, the ionic silver clusters reduce to neutral ones and move toward the surface. Simultaneously, due to the external electric field the clusters interact with other ones as induced electrical dipoles. This leads to alignment of nanoparticles along $\vec{E}_0$ and formation of a chain-like conductive structure, which makes the sample dichroic. Taking into account the matrix surface viscosity and using the method of image dipoles to model the influence of the substrate on the dipole interactions, we give an interpretation about the relative equilibrium positions of generated nanoclusters and consequently the formation mechanism of the chain-like structure on the surface of the ion-exchanged glass.

1 Introduction

Ion-exchanged glass is one of the most investigated optical materials, because of its interesting optical properties especially, waveguide applications [1–5] and simplicity of its preparation methods [6]. It is also a very convenient environment for producing metallic nanoparticles and obtaining determined optical properties. Profiling the index of refraction [7], functioning as a slab waveguide [4–6, 8, 9], changes in the absorption [10, 11] and fluorescence spectra [12, 13] are some of the important reported results.

On the other hand, ordering the produced metallic nanoparticles could give new properties to the samples and has many applications, such as making diffraction gratings [14], optical information recording [15, 16], sensitivity to light polarization and induced dichroism [17–20].

Silver ion-exchanged glass has been used as the matrix and the produced nanoclusters were aligned on its surface with two different methods: (i) by interaction with a linearly polarized Ar^+ laser beam [19]; and (ii) by interaction with an external uniform DC electric field parallel to the sample's surface [20]. In both cases the produced silver nanoparticles were aligned along the external electric field $\vec{E}_0$. This ordering makes the samples dichroic, which means that the absorption spectra for a linearly polarized probe beam, $\vec{E}$, are different for two orthogonal states of its polarization (that is, for $\vec{E} \parallel \vec{E}_0$ and $\vec{E} \perp \vec{E}_0$). Heating the ion-exchanged glass results in reducing some of its ionic silver clusters to neutral ones and increases their mobility [11, 21, 22]. The temperature increase of the samples could be exerted by laser irradiation or by heating in an oven. Previously, a motion of produced neutral nanoclusters toward the surface of the samples, during the heating, was reported [9, 20, 23–25]. On the other hand, the produced hot mobile clusters prefer to continue aggregation, since it is an exothermic process [11]. Simultaneously, on the surface of the samples the generated neutral silver clusters interact with the external electric field $\vec{E}_0$ and become electric dipoles. The dipole–dipole interaction leads to the alignment of the silver nanoparticles and formation of a chain-like structure along $\vec{E}_0$ [19, 20].

A. Nahal (✉) · R. Talebi
Photonic Materials Research Laboratory, Department of Physics, University of Tehran, 14399-55961 Tehran, Iran
e-mail: nahal@khayam.ut.ac.ir
Fax: +98-21-88004781

R. Talebi
e-mail: talebi_razieh@yahoo.com

M. Miri
Department of Physics, University of Tehran, 14399-55961 Tehran, Iran
e-mail: miri@iasbs.ac.ir

In the present article, we have tried to address the following question: what are the parameters playing essential roles in the determination of the produced structure, and how are the produced silver nanoparticles ordered along $\vec{E}_0$?

2 Experiments and results

2.1 Sample preparation

Samples are prepared by the well-known ion-exchange method. In this method a soda-lime glass substrate (0.8 mm $\times$ 10 mm $\times$ 20 mm) is placed in a molten mixture of $AgNO_3$ and $NaNO_3$ salts, with determined portions of each one (in our case: 4 wt % $AgNO_3$ and 96 wt % $NaNO_3$ (wt %: weight percent), at high temperature $T' = 400°C$). As a result, some of the silver ions of the mixed molten salt would exchange with some of the sodium ions of the soda-lime glass matrix, via thermal diffusion [6]. The diffused silver ions could form ionic silver clusters, Ag_N^+ [11], where N is the number of the atoms forming the cluster.

On the basis of XRF (X-Ray Fluorescence) analysis, the glass used in our experiments has the following composition: 73.72 wt % SiO_2, 6.98 wt % CaO, 12.9 wt % Na_2O, 4.08 wt % MgO, 0.353 wt % Al_2O_3, 0.10 wt % K_2O, 0.135 wt % Cl, 0.07 wt % Fe_2O_3 and 1.653 wt % SO_3. Duration time, the temperature at which the ion-exchange process is performed and amount of the $AgNO_3$ in the mixed molten salt are the most important parameters determining the diffusion depth and the concentration of the ionic silver clusters in the glass substrate.

In order to prepare a one-side ion-exchanged sample, the precisely cleaned surface of the glass substrate was covered uniformly by a very fine homogeneous powder of the mixed salt. Afterwards, the sample was placed in an electrical oven ($T'_{max} = 1200°C$) at temperature $T' = 400°C$ for 2 h. Therefore, the powder of the mixed salts melts and the ion-exchange process begins. About 30 min is enough to obtain an ion-exchanged glass. Longer process results in thermal reduction of ionic silver clusters to neutral ones. In [21] it was shown that there is no simple linear relation between the ion-exchange duration time, size and distribution of the produced clusters. Non-binding oxygen in the glass matrix [26], Fe_2O_3 impurity in the glass [27] and the surrounding atmosphere are the sources of electrons for reducing the heated ionic Ag_N^+ clusters to the neutral ones.

2.2 Inducing dichroism by ordering the silver nanoparticles

In the first part of this study [20], we placed the ion-exchanged glass between two plates of a capacitor (Fig. 1 of [20]) and simultaneously heated the sample in the presence of a uniform high voltage DC electric field $\vec{E}_0$ (produced by the capacitor), parallel to its surface. Repeating the reported experiment in [20], we observed that the growing silver nanoparticles are aligned along $\vec{E}_0$ on the surface of the sample (Fig. 1). That is, the forming neutral silver clusters interact with $\vec{E}_0$ and become dipoles [19, 20]. Aggregation of such dipoles, under the action of $\vec{E}_0$, results in their arrangement along $\vec{E}_0$ and formation of a chain-like structure. As Fig. 1 shows, the range of the size of the larger nanoparticles is mainly between 40 nm and 60 nm and the average distance between them is mostly about 500 nm.

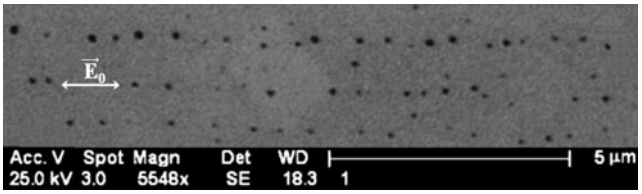

Fig. 1 The SEM image of ordered silver nanoparticles on the surface of the ion-exchanged glass, after the thermo-electric treatment

Such induced ordering of metallic nanoparticles makes the sample dichroic. In other words, the optical density, D ($D = -\log T$, where T is the transmittance of the sample), is different for two cases: the optical density $D_{\parallel}$ when the polarization of the probe beam is parallel to $\vec{E}_0$ is more than the optical density $D_{\perp}$ when the polarization is perpendicular to $\vec{E}_0$. Our ion-exchanged samples were placed for 2 h at temperature $T' = 400°C$ in the electric field $\vec{E}_0 = 1$ kV/cm. We have measured dichroism $\Delta D = D_{\parallel} - D_{\perp}$ for our samples (Fig. 2). It was previously found [21] that increasing of the ion-exchange duration time is accompanied by variation of amount and size of the neutral silver nanoparticles. In [21], it was shown that after 1.5 h of ion exchanging the size of the produced cluster is about its maximum value. Our measurements show that at 1.5 h of ion exchanging the amount of dichroism ΔD reaches its maximum value for our samples (Fig. 2b). On the other hand, the amount of ΔD depends on the concentration of the silver clusters in the glass matrix [19]. Thus, the above-mentioned results in both studies are consistent.

3 Discussion

In this part we try to address the questions related to the forming mechanism of the produced structure.

3.1 Formation of the chain-like structure

With increasing temperature of ion-exchanged glass, the mobility of the ionic silver clusters increases and reduction to the neutral ones begins. At the same time, the neutral clusters start to move toward the surface of the glass matrix [9, 20, 23–25]. As the viscosity of the glass matrix is high,

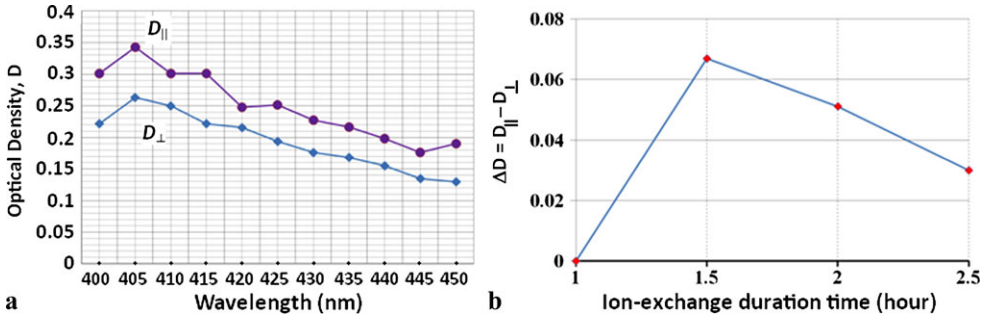

Fig. 2 (**a**) Absorption spectra of 1.5 h ion-exchanged sample after thermo-electric treatment for two orthogonal polarization states; (**b**) variation of induced dichroism vs. ion-exchange duration time

moving clusters need time to reach the surface and prefer to aggregate on the surface rather than the interior of the matrix. On the other hand, the static dielectric constant of glass, $k_{\text{glass}} = \frac{\varepsilon_g}{\varepsilon_0} \sim 42$ [28], has a large value (where ε_g and ε_0 are absolute permittivities of glass and air, respectively). Thus, the electric field $\vec{E}_{\text{inside}} = \vec{E}_0/k_{\text{glass}}$ is too weak inside the glass matrix. Therefore, $\vec{E}_{\text{inside}}$ is not able to convert efficiently a formed cluster, moving toward to the surface, to a dipole. That is, due to high dielectric constant and high viscosity of the matrix, aggregation of the produced neutral clusters and converting them to the dipoles and their simultaneous arrangement under the action of $\vec{E}_0$ via dipole–dipole interaction could happen chiefly on the surface of the sample.

Now, for those clusters which are on the surface and are aggregating, the electric field $\vec{E}_0$ is strong enough to make them dipoles. As shown in [19, 20], dipole–dipole interaction of the clusters results in their arrangement, mainly, along the direction of the uniform $\vec{E}_0$ (Fig. 1). In other words, the generated dipoles prefer to attract each other along $\vec{E}_0$ and repulse each other along the direction perpendicular to $\vec{E}_0$. This leads to formation of larger clusters which are a little prolated along $\vec{E}_0$. In such a way, the chain-like structure of silver nanoparticles could be produced along $\vec{E}_0$.

3.2 The role of image of dipoles

We model a cluster as an ellipsoid with dimensions a, b and c. Due to the electric field $\vec{E}_0$, the cluster acts as a dipole. For each generated dipole on the surface of the sample we can write [29]

$$\vec{P} = 4\pi\varepsilon_0 abc\left(\frac{\varepsilon_{\text{Ag}} - \varepsilon_0}{3L_x\varepsilon_{\text{Ag}} + (3 - 3L_x)\varepsilon_0}\right)\vec{E}_0, \tag{1}$$

where ε_{Ag} is the dielectric constant of silver and L_x is a geometrical coefficient, which is related to the ellipticity of the cluster. As a first-order approximation, we model our particles as oblate ellipsoids. Thus, we write $a = b = R$ and $c = \xi R$, where ξ is a coefficient which determines how our particle differs from a sphere.

Dipoles on the dielectric substrate (the ion-exchanged glass matrix) are accompanied by their image dipoles [29]

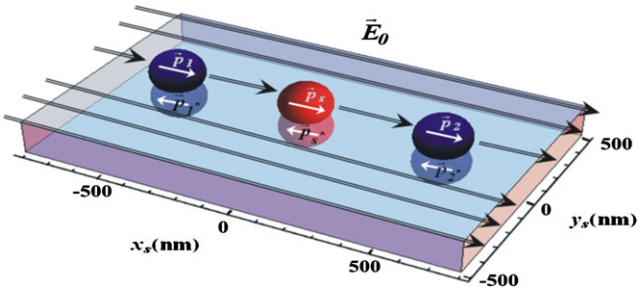

Fig. 3 Schematic image of three aligned clusters on the surface of sample. $\vec{P}_j^*$ is the image of dipole $\vec{P}_j$

(Fig. 3). The image dipole $\vec{P}^*$ of a dipole $\vec{P}$, parallel to the surface of the glass, is

$$\vec{P}^* = -\left(\frac{\varepsilon_g - \varepsilon_0}{\varepsilon_g + \varepsilon_0}\right)\vec{P}, \tag{2}$$

where ε_g is the dielectric constant of the glass matrix. Since $\frac{\varepsilon_{\text{Ag}}}{\varepsilon_0} \gg 1$ [30], we have

$$\vec{P} \simeq \frac{4\pi\varepsilon_0\xi R^3}{3L_x}\vec{E}_0. \tag{3}$$

Focusing on the sth particle of a chain (Fig. 1), we take into account the dipole–dipole interaction of all neighboring silver nanoparticles. First we find the total potential energy of the chain and then using the relation between the force and potential energy: $\vec{F} = -\vec{\nabla}U$, we calculate the force exerted on the sth particle. The total electric potential for the sth particle consists of three terms:

(i) Interaction between the sth particle and the jth particle of the chain [29]:

$$U_{sj} = \frac{1}{4\pi\varepsilon_0}\left[\frac{\vec{P}_s\cdot\vec{P}_j}{|r_s - r_j|^3} - \frac{3}{|r_s - r_j|^5}\left[\vec{P}_s\cdot(\vec{r}_s - \vec{r}_j)\right] \times\left[\vec{P}_j\cdot(\vec{r}_s - \vec{r}_j)\right]\right]. \tag{4}$$

(ii) Interaction between the sth particle and the image of the jth particle of the chain:

$$U_{sj^*} = \frac{1}{4\pi\varepsilon_0}\left[\frac{\vec{P}_s\cdot\vec{P}_{j^*}}{|r_s - r_{j^*}|^3} - \frac{3}{|r_s - r_{j^*}|^5}\left[\vec{P}_s\cdot(\vec{r}_s - \vec{r}_j^*)\right]\right.$$

$$\times \left[\vec{P}_{j^*} \cdot \left(\vec{r}_s - \vec{r}_{j^*}\right)\right]\Bigg]. \tag{5}$$

Note that the image $\vec{P}_{j^*}$ of a dipole $\vec{P}_j$ at $\vec{r}_j = (x_j, y_j, z_j)$ resides at $\vec{r}_{j^*} = (x_j, y_j, -z_j)$.

(iii) Interaction between the sth particle and its image:

$$U_{ss^*} = \frac{1}{4\pi\varepsilon_0}\Bigg[\frac{\vec{P}_s \cdot \vec{P}_{s^*}}{|r_s - r_{s^*}|^3} - \frac{3}{|r_s - r_{s^*}|^5}\left[\vec{P}_s \cdot \left(\vec{r}_s - \vec{r}_{s^*}\right)\right] \times \left[\vec{P}_{s^*} \cdot \left(\vec{r}_s - \vec{r}_{s^*}\right)\right]\Bigg]. \tag{6}$$

Thus, the total potential energy which the sth particle of the chain feels is equal to

$$U_s = U^s_{\text{total}} = \sum_j U_{sj} + \sum_{j^*} U_{sj^*} + U_{ss^*}. \tag{7}$$

To draw properly the variation of potential energy, we introduce the normalization energy as

$$U_0 = \frac{1}{4\pi\varepsilon_0}\frac{P_0^2}{\ell^3} \quad \text{with } P_0 = \frac{4\pi\varepsilon_0\xi R_0^3}{3L_x}E_0, \tag{8}$$

where P_0 is a typical dipole moment and ℓ is a typical length. We choose $R_0 = 50$ nm, $L_x = 0.04$, $\ell = 5$ nm, $\xi = 0.1$ and $\vec{E}_0 = 1$ kV/cm, on the basis of experimental data (Fig. 1). Hence, we obtain $U_0 = 9.65 \times 10^{-20}$ J. We also introduce scaled parameters as

$$\hat{\vec{P}}_j = \frac{\vec{P}_j}{P_0}; \qquad \hat{\vec{r}}_j = \frac{\vec{r}_j}{\ell}; \qquad \hat{x}_j = \frac{x_j}{\ell}. \tag{9}$$

Using the scaled parameters for three particles in which the sth particle is placed at the middle between two other similar ones, we can rewrite U_s as

$$\begin{aligned}\frac{U_S}{U_0} = \left|\hat{\vec{P}}_s\right|\left|\hat{\vec{P}}_1\right|\Bigg\{&\Bigg[\frac{1}{|\hat{\vec{r}}_s - \hat{\vec{r}}_1|^3} - \frac{3(\hat{x}_s - \hat{x}_1)^2}{|\hat{\vec{r}}_s - \hat{\vec{r}}_1|^5} \\ &+ \frac{1}{|\hat{\vec{r}}_s - \hat{\vec{r}}_2|^3} - \frac{3(\hat{x}_s - \hat{x}_2)^2}{|\hat{\vec{r}}_s - \hat{\vec{r}}_2|^5}\Bigg] \\ &- \left(\frac{\varepsilon_g - \varepsilon_0}{\varepsilon_g + \varepsilon_0}\right)\Bigg[\frac{1}{|\hat{\vec{r}}_s - \hat{\vec{r}}_{1^*}|^3} - \frac{3(\hat{x}_s - \hat{x}_1)^2}{|\hat{\vec{r}}_s - \hat{\vec{r}}_{1^*}|^5} \\ &+ \frac{1}{|\hat{\vec{r}}_s - \hat{\vec{r}}_{2^*}|^3} - \frac{3(\hat{x}_s - \hat{x}_2)^2}{|\hat{\vec{r}}_s - \hat{\vec{r}}_{2^*}|^5}\Bigg] \\ &- \left(\frac{\varepsilon_g - \varepsilon_0}{\varepsilon_g + \varepsilon_0}\right)\Bigg[\frac{1}{|\hat{\vec{r}}_s - \hat{\vec{r}}_{s^*}|^3} - \frac{3(\hat{x}_s - \hat{x}_{s^*})^2}{|\hat{\vec{r}}_s - \hat{\vec{r}}_{s^*}|^5}\Bigg]\Bigg\}. \end{aligned} \tag{10}$$

Now, we plot the variation of U_s/U_0 vs. x_s/ℓ (normalized position along the connecting line of two neighboring particles, where x_s is the coordinate of the sth particle). The results of our calculation for two cases: (i) when the image dipoles are excluded; and (ii) when image dipoles are included in the calculation are shown in Fig. 4, curves a and b, respectively. Figure 4 shows that, for the case (ii) the absolute value of potential energy is higher. Later, we will show that force calculations for the two above-mentioned cases

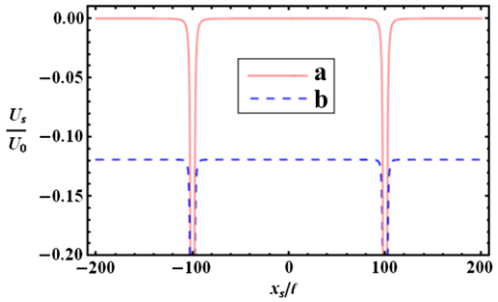

Fig. 4 Normalized total interaction energy U_s/U_0 between two neighboring particles vs. normalized distance x_s/ℓ: (**a**) without image dipoles; (**b**) with image dipoles

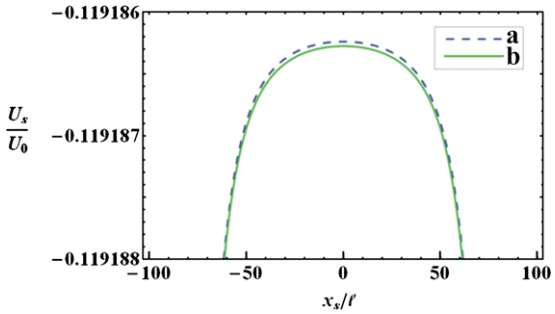

Fig. 5 Normalized total potential energy including image dipoles, (**a**) taking into account three particles of the chain; (**b**) taking into account 21 particles of the chain, in the space between two neighboring ones

indicate that a wider range with a slowly varying function of the force acting on the sth particle would be obtained for the case when the image dipoles are included in the calculation.

Our numerical calculations for potential energy of the sth particle are shown in Fig. 5, for cases when we take into account just two closest neighbors (curve a) and when we take into account the next 20 particles (curve b), which make the chain-like structure in Fig. 1. Note that curve a of Fig. 5 is the enlarged part of curve b of Fig. 4, where U_s/U_0 is a slowly varying function of x_s/ℓ. From Fig. 5 it is clear that the two closest neighboring particles and their images have a dominant influence on shaping the potential in the space between closest neighbors, and farther neighboring particles of the chain have no essential influence on the shape of the potential. On the basis of the scanning electron microscope (SEM) image (Fig. 1), in both calculations the average distance between neighboring clusters is taken as 500 nm. Figure 5 shows that the equilibrium of the sth particle between its two neighboring particles is *unstable*, but there is a wide range space along the x axis between the two particles, where the sth particle could stay there almost stably and participate in forming the chain-like structure.

Taking into account the image dipoles, a plot of the potential energy for two closest neighbors of the sth particle is

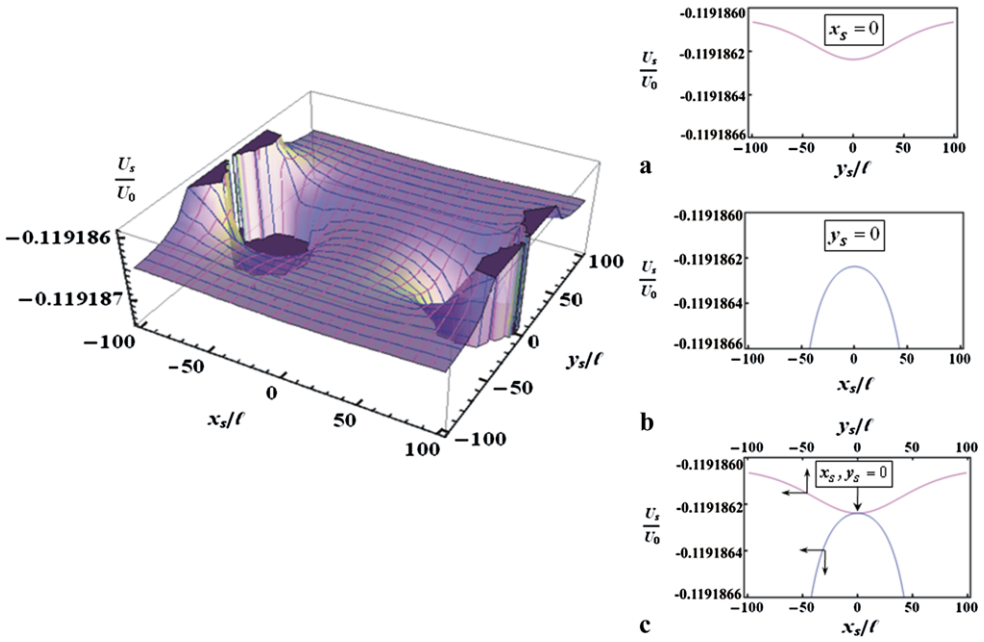

Fig. 6 Potential energy diagram: (**a**) its variation along y axis; (**b**) its variation along x axis; (**c**) both variations shown in one diagram

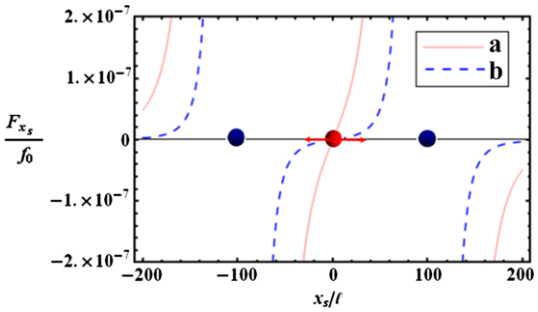

Fig. 7 Normalized electrical force acting on the sth particle for: (a) the case where image dipoles are excluded; (b) the case where image dipoles are included in the calculation

shown in Fig. 6. Also, cross sections of potential energy in directions of x and y axes are shown. Quite interestingly, inset (a) in Fig. 6 shows that, along the y axis, also we have a minimum in the potential energy which assists the particles to remain along the chain-like structure. It is clear that the shape of the potential energy along the y axis leads to existence of a restoring force, which pushes back the sth particle toward the connecting line of the chain. Along the x axis the potential energy has an unstable equilibrium, which causes that even with a small perturbation the sth particle would be absorbed by the closest neighbor.

As was mentioned, the image dipoles influence the resultant relative equilibrium position of the sth particle between two neighboring nanoparticles. In this connection, we have calculated the force acting on the sth particle:

$$F_{x_s} = -\frac{\partial U_s}{\partial(x_s)}. \tag{11}$$

We introduce the typical force

$$f_0 = \frac{1}{4\pi\varepsilon_0}\frac{P_0^2}{\ell^4} = 1.93 \times 10^{-11}\ \text{N}. \tag{12}$$

Therefore, we draw the variation of normalized $\frac{F_{x_s}}{f_0}$ vs. $\frac{x_s}{\ell}$ in the absence (Fig. 7, curve a) and in the presence of the image dipoles (Fig. 7, curve b). From Fig. 7 it is apparent that, taking into account the image dipoles, F_{x_s} is a more slowly varying function of $\frac{x_s}{\ell}$ in comparison to the case when the image dipoles are excluded. Accordingly, by taking into account the image dipoles, a larger space for the relative equilibrium position, in which the sth particle could participate in formation of the chain-like structure, is available.

3.3 The role of surface viscosity of the ion-exchanged glass

The electrostatic forces acting on the sth silver nanoparticle (the probe particle) due to dipole–dipole interaction with neighboring ones are not sufficient to explain the physics of the system. If we assume that a silver nanoparticle moving on the surface of the matrix is slightly floating, a resistance force also acts on it. This force is related to the surface viscosity of the ion-exchanged glass matrix. Thus, the total force acting on each induced dipole equals

$$\sum \vec{F} = \vec{F}_{\text{electrical}} + \vec{F}_{\text{surface viscosity}} = m\vec{a}, \tag{13}$$

where m is the mass of the dipole and $\vec{a}$ is its acceleration.

Generally, the dragging force is related to the velocity $\vec{v}$ of the moving silver nanoparticles as follows [31]:

$$\vec{F}_{\text{surface viscosity}} = -c_{\text{d}}\vec{v}, \tag{14}$$

where c_{d} is the drag constant and characterizes the *surface* viscosity of the glass matrix.

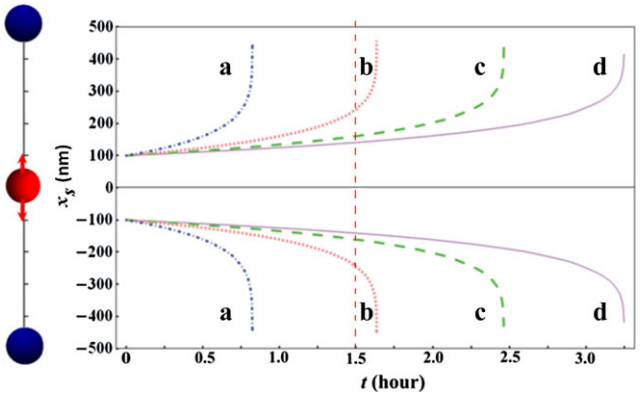

Fig. 8 Variation of position of the sth cluster vs. time, for different assumed surface viscosities of the sample: $a = 0.5 \times 10^{-8}$ N s/m, $b = 1 \times 10^{-8}$ N s/m, $c = 1.5 \times 10^{-8}$ N s/m, $d = 2 \times 10^{-8}$ N s/m

On the basis of experimental results (Fig. 1), we take the shape of produced clusters as oblate ellipsoids with $R_1 = R_2 = R = 50$ nm, $\xi = 0.1$, so $R_3 = \xi R = 5$ nm, $L_x = 0.04$ and average distance between neighbors $d = 500$ nm. We assume $\varepsilon_g = 42\varepsilon_0$ [28], $m = \frac{4}{3}\pi\xi R^3 \rho_{Ag}$ with $\rho_{Ag} = 10.49 \times 10^3$ kg/m^3 [32]. Thus, solving (13) for $x_s(t)$ gives us an estimate about the order of magnitude of the surface viscosity of the heated ion-exchanged glass for moving silver nanoparticles.

We plot changes of x_s vs. time t (the duration time of the thermo-electric treatment) for different assumed surface viscosities (Fig. 8). In this way, we could argue about the time after which destruction of the generated chain-like structure initiates. Any perturbation in position of the clusters from the relative equilibrium range leads to agglomeration of the clusters and destruction of the induced structure. From Fig. 8 we can conclude that for the sample with $t = 1.5$ h, the surface viscosity of the glass matrix is about 1.5×10^{-8} N s/m. Hence, our model predicts that further increasing the duration time of the thermo-electric treatment results in particle aggregation and consequently disappearance of induced dichroism. This is in agreement with experimental observations [20].

These results indicate that in the high-viscosity regime ordering of silver nanoparticles does not happen. On the other hand, very low surface viscosity also results in agglomeration of the produced clusters in first minutes of the process and no stable chain-like structure could be produced. An intermediate viscosity range gives time for clusters to be ordered along $\vec{E}_0$ to form the chain-like structure and induce the dichroism property.

4 Conclusion

By using a high voltage uniform DC electric field $\vec{E}_0$ parallel to the surface of heated ion-exchanged glasses dichroism is induced, due to ordering of produced silver nanoparticles along $\vec{E}_0$. The mechanism of this experiment is investigated. It is found that heating the ion-exchanged glass results in formation of neutral silver clusters on its surface. The presence of $\vec{E}_0$ converts clusters to dipoles. The dipole–dipole interaction of nearest particles aligns them along $\vec{E}_0$ and a chain-like structure forms on the surface of the samples. Since absorption along the chain is higher than in the direction perpendicular to the chain, dichroism is thus induced.

Results of our studies indicate that the image dipole of each cluster (dipole) should be taken into account for determination of relative equilibrium positions of particles participating in formation of the chain. On the other hand, we found that an intermediate surface viscosity range (order of 10^{-8} N s/m) sets up the condition for stable generation of the structure and, consequently, induction of dichroism.

References

1. P. Chakraborty, J. Mater. Sci. **33**, 2235 (1998)
2. F. Gonella, P. Mazzoldi, *Handbook of Nanostructured Materials and Nanotechnology* (Academic Press, San Diego, 2000)
3. R. Rangel-Rojo, J.A. Reyes-Esqueda, C. Torres-Torres, A. Oliver, L. Rodriguez-Fernandez, A. Crespo-Sosa, J.C. Cheang-Wong, J. McCarthy, H.T. Bookey, A.K. Kar, in *Silver Nanoparticles*, ed. by Pozo, D., (InTech, Rijeka, 2010). ISBN: 978-953-307-028-5. Available from: http://www.intechopen.com/articles/show/title/linear-and-nonlinear-optical-properties-of-aligned-elongated-silver-nanoparticles-embedded-in-silica
4. A. Tervonen, B.R. West, S. Honkanen, Opt. Eng. **50**, 071107 (2011)
5. S. Honkanen, B.R. West, S. Yliniemi, P. Madasamy, M. Morrell, J. Auxier, A. Schülzgen, N. Peyghambarian, J. Carriere, J. Frantz, R. Kostuk, J. Castro, D. Geraghty, Phys. Chem. Glasses **47**, 110 (2006)
6. S.I. Najafi, *Introduction to Glass Integrated Optics* (Artech House, Norwood, 1992)
7. J.L. Jackel, Appl. Opt. **27**, 472 (1988)
8. C.R. Lavers, K. Itoh, S.C. Wu, M. Murabayashi, I. Mauchline, G. Stewart, T. Stout, Sens. Actuators B **69**, 85 (2000)
9. E. Borsella, G. De Marchi, F. Caccavale, F. Gonella, G. Mattei, P. Mazzoldi, G. Battaglin, A. Quaranta, A. Miotello, J. Non-Cryst. Solids **253**, 261 (1999)
10. G. Battaglin, E. Borsella, G. De Marchi, F. Gonella, G. Mattei, P. Mazzoldi, A. Quaranta, Proc. SPIE **3405**, 533 (1997)
11. U. Kriebig, M. Vollmer, *Optical Properties of Metal Clusters* (Springer, Berlin, 1995)
12. A. Nahal, H.R.M. Khalesifard, Opt. Mater. **29**, 987 (2007)
13. M. Weisser, F. Thoma, B. Menges, U. Langbein, S. Mittlerneher, Opt. Commun. **153**, 27 (1998)
14. L.A. Ageev, V.K. Miloslavsky, Opt. Eng. **34**, 960 (1995)
15. L.A. Ageev, V.K. Miloslavsky, A. Nahal, J. Opt. A, Pure Appl. Opt. **1**, 173 (1999)
16. http://www.faqs.org/patents/app/20080230826
17. L.A. Ageev, V.K. Miloslavsky, A. Nahal, Pure Appl. Opt. **7**, L1 (1998)
18. V.K. Miloslavsky, A. Nahal, L.A. Ageev, Opt. Commun. **147**, 436 (1998)
19. A. Nahal, H.R.M. Khalesifard, J. Mostafavi-Amjad, Appl. Phys. B **79**, 513 (2004)
20. A. Nahal, K. Shapoori, Appl. Surf. Sci. **255**, 7946 (2009)

21. A. Nahal, A. Jalehdoost, Kh. Hassani, A. Farokhniaee, Eur. Phys. J. Appl. Phys. **53**, 10701 (2011)
22. F. Gonella, G. Mattei, P. Mazzoldi, E. Cattaruzza, G.W. Arnold, G. Battaglin, P. Calvelli, R. Polloni, B. Bertonecello, R.F. Haglund Jr., Appl. Phys. Lett. **69**, 3101 (1996)
23. M. Miotello, M. Bonelli, G. De Marchi, G. Mattei, P. Mazzoldi, C. Sada, F. Gonella, Appl. Phys. Lett. **79**, 2456 (2001)
24. A. Nahal, J. Mostafavi-Amjad, A. Ghods, M.R.H. Khajehpour, S.N.S. Reihani, M.R. Kolahchi, J. Appl. Phys. **100**, 053503 (2006)
25. A.L. Stepanov, V.N. Popok, D.E. Hole, A.A. Bukharaev, Phys. Solid State **43**, 2192 (2001)
26. C. Mohr, M. Dubiel, H. Hofmeister, J. Phys., Condens. Matter **13**, 525 (2001)
27. A. Berger, J. Non-Cryst. Solids **151**, 88 (1992)
28. M. Tomozawa, J.F. Cordaro, M. Singh, J. Non-Cryst. Solids **40**, 189 (1980)
29. J.D. Jackson, *Classical Electrodynamics* (Wiley, New York, 1999)
30. S.K. Saha, Phys. Rev. B **69**, 125416 (2004)
31. G.K. Batchelor, *An Introduction to Fluid Dynamics* (Cambridge University Press, London, 1967)
32. N.N. Greenwood, A. Earnshaw, *Chemistry of the Elements* (Pergamon, Oxford, 1984)